JCTC Journal of Chemical Theory and Computation

Mapping All-Atom Models onto One-Bead Coarse-Grained Models: General Properties and Applications to a Minimal Polypeptide Model

Valentina Tozzini*

NEST − Scuola Normale Superiore, Piazza dei Cavalieri, 7 I-56126 Pisa, Italy

Walter Rocchia

Scuola Normale Superiore, Piazza dei Cavalieri, 7 I-56126 Pisa, Italy

J. Andrew McCammon

Department of Chemistry and Biochemistry, Center for Theoretical Biological Physics, Howard Hughes Medical Institute, Department of Pharmacology, University of California at San Diego, La Jolla, California 92093

Abstract: In the one- and two-bead coarse-grained (CG) models for proteins, the two conformational dihedrals ϕ and ψ that describe the backbone geometry are no longer present as explicit internal coordinates; thus, the information contained in the Ramachandran plot cannot be used directly. We derive an analytical mapping between these dihedrals and the internal variable describing the backbone conformation in the one- (two-) bead CG models, namely, the pseudo-bond angle and pseudo-dihedral between subsequent Cα's. This is used to derive a new density plot that contains the same information as the Ramachandran plot and can be used with the one- (two-) bead CG models. The use of this mapping is then illustrated with a new one-bead polypeptide model that accounts for transitions between α helices and β sheets.

1. Introduction

Coarse-grained (CG) models for proteins have become more and more popular in the past two decades, because of the necessity of simulating systems on the size scale of hundreds of nanometers and on the time scale of microseconds.[1,2] The seminal concept can be traced back to the 1970s:[3,4] these simplified models for proteins are based on united-atom representations using one to six interacting centers (beads) for each amino acid. Four- to six-bead models represent explicitly the backbone atoms [Cα, N(H), and C(O)] with additional "beads" for the side chain and for the backbone carbonylic oxygen and the backbone hydrogen,[5−7] and they use the ϕ and ψ dihedrals formed by the backbone atoms C−N−Cα−C and N−Cα−C−N, respectively, as internal variables. Conversely, in one- (two-) bead models, only the Cα (and additional beads for the side chain) is (are) explicitly present (see Figure 1).

The two-dimensional density plot of ϕ and ψ referring to a given Cα is called the Ramachandran map. This map is more dense in specific regions of the ϕ,ψ plane, each pertaining to a particular secondary structure. Other regions are "forbidden" because of the steric hindrance of the backbone atoms. Thus, the Ramachandran plot is a simple and immediate tool to check the reliability of a model protein. But, while this check can be directly done in four- (to six-) bead models, this is no longer possible in the one- (two-) bead models. In fact, in these models, the ϕ and ψ are no longer explicit internal variables and the description of the backbone geometry relies on different internal variables, that is, the Cα−Cα−Cα angle θ and the Cα−Cα−Cα−Cα dihedral α (see Figure 1). So far, the problem of how to

* Corresponding author fax: +39-050-509417; e-mail: tozzini@nest.sns.it.
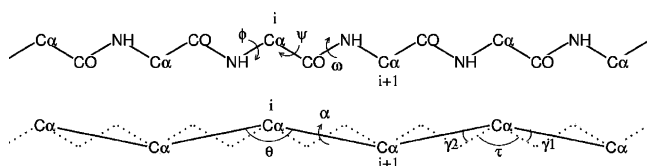
Figure 1. Schematic representation of the coarse-graining procedure. The internal coordinates (ϕ, ψ, ω) and θ,α and the angles defining the CG geometry (τ, $\gamma1$, $\gamma2$) are reported.

transfer the information contained in the Ramachandran plot to these simplified models has not been given any consideration. This is quite surprising, given the fact that one- and two-bead models have recently undergone rapid developments, becoming more accurate and sophisticated.[8−15]

In this paper, we derive an analytical correspondence of the all-atom internal backbone coordinates (ϕ,ψ) to the CG internal backbone coordinates (α,θ) that allows one to explicitly map the Ramachandran plot onto a new θ,α conformational density plot. The force field (FF) of the recent one- and two-bead CG models are reconsidered on the basis of the θ,α map. As an illustration of these concepts, a new one-bead model for polypeptides is presented that accounts for helix to sheet secondary structure transitions.

2. Coarse Graining and Mapping of the Internal Backbone Coordinates

The procedure leading from an all-atom model to a one-(two-) bead CG model is schematically described in Figure 1. The bond length and the backbone bond angle NH−Cα−CO display only small variations from the average values ($\tau = 111°$), and the peptide bond geometry is planar ($\omega = 180$), implying that the dihedral angles ϕ and ψ are basically the only free internal variables. [In this paper, we neglect the (rare) possibility of a cis conformation of the peptide bond ($\omega = 0$).] In the CG description, the backbone conformation is determined by the bond angle between three subsequent Cα's and the dihedral between four subsequent Cα's. The bond angle with vertex Cα_i, (θ_i) depends only on the two adjacent dihedrals ϕ_i and ψ_i, whereas the dihedral between Cα_{i-1} and Cα_{i+2}, namely, $\alpha_{i,i+1}$, depends on the four dihedrals ϕ_i, ψ_i, ϕ_{i+1}, and ψ_{i+1}. Both θ and α depend parametrically on τ and on the two angles between the bonds Cα−Cα and Cα−CO or Cα−NH, which for the trans conformation assume the almost constant values of $\gamma1 = 20.7°$ and $\gamma1 = 14.7°$, respectively (see Figure 1 for the definition of angles and dihedrals). The angle θ as a function of ϕ,ψ is given by the following formula (valid for the trans conformation):

$$\cos(\theta_i) = \cos(\tau)[\cos(\gamma1)\cos(\gamma2) -$$
$$\sin(\gamma1)\sin(\gamma2)\cos(\phi_i)\cos(\psi_i)] -$$
$$\sin(\gamma1)\sin(\gamma2)\sin(\phi_i)\sin(\psi_i) +$$
$$\sin(\tau)[\cos(\psi_i)\sin(\gamma1)\cos(\gamma2) +$$
$$\cos(\phi_i)\cos(\gamma1)\sin(\gamma2)] \quad (1)$$

For (ϕ, ψ) = (180, 180), (0, 0), (180, 0), and (0, 180), one has $\theta = \tau + (\gamma1 + \gamma2)$, $\theta = \tau - (\gamma1 + \gamma2)$, $\theta = \tau + (\gamma1 - \gamma2)$, and $\theta = \tau - (\gamma1 - \gamma2)$, respectively. The first

corresponds to the completely extended conformation; the others are planar but sterically forbidden or weakly allowed conformations (see below). The exact formula giving α explicitly as a function of the ϕ,ψ dihedrals is very complex; however, a precision of a few percent can already be obtained at the linear order in $\gamma1$ and $\gamma2$ (see the Supporting Information):

$$\alpha_{i,i+1} = 180 + \psi_i + \phi_{i+1} + \gamma1\sin(\psi_{i+1}) + \gamma2\sin(\phi_i) \quad (2)$$

This formula (with $\gamma1 = \gamma2$) was previously reported by Levitt.[3]

To make general considerations, we restrict ourselves to the case $\gamma1 = \gamma2$. Furthermore, we assume that the geometrical properties are uniform along the chain (or, equivalently, we consider cases of well-defined secondary structure), so that we can put $\phi_i = \phi_{i+1}$ and $\psi_i = \psi_{i+1}$ and drop the dependence on the index $i + 1$ in eq 2. In these conditions, the map (ϕ, ψ) → (α, θ) is symmetric under the exchange $\phi \leftrightarrow \psi$. Thus, the upper triangle in the (ϕ, ψ) plane is superimposed upon folding along the main diagonal (in magenta) over the lower triangle and mapped onto the same region in the α,θ plane. The periodicity and the additional symmetry $\theta(\phi, \psi) = \theta(-\phi, -\psi) = \theta(\phi + 180, \psi + 180)$ determine the peculiar "butterfly" shape of the image of the ϕ,ψ plane in the α,θ plane reported in Figure 2. In the general case when $\gamma1 \neq \gamma2$, the $\phi \leftrightarrow \psi$ symmetry is slightly broken and one has two slightly different "butterfly" images superimposed. It is to be noted that, as the whole α axis is spanned, the θ angle can assume only values ranging between $\tau - \gamma1 - \gamma2$ and $\tau + \gamma1 + \gamma2$, corresponding to the planar-contracted (forbidden) configuration ($\phi = \psi = 0$) and the planar extended configuration ($\phi = \psi = 180$). As the angle α approaches the value 0, the allowed range for θ becomes smaller. Ring structures correspond to $\alpha = 0$: the maximum value for θ is $\tau = 111 + |\gamma2 - \gamma1|$, obtained for $\phi = 180°$ and $\psi = 0°$, corresponding roughly to a six-membered ring, while the minimum value for θ is ∼105°, obtained for $\phi = \psi \simeq \pm75°$, corresponding roughly to a five-membered ring.

3. Conversion of the Ramachandran Plot into the α,θ Plot

We use the above relationships to convert the Ramachandran plot into a conformational density plot in the α,θ plane. The conversion for the generic Ramachandran plot and the Ramachandran plots of glycine, proline, and pre-proline residues are reported in Figure 3.

We observe that the symmetry-induced folding of the ϕ,ψ plane along the diagonal produces some peculiarities of the α,θ conformational maps. For instance, the forbidden region around $\phi = \psi = 0$ (simplified as a circle in Figure 3) is folded onto itself and mapped onto a flat region around $\alpha = \pm180°$, $\theta = \tau - \gamma1 - \gamma2 = \simeq75°$. Conversely, the forbidden region around $\phi = 0$, $\psi = \pm180°$ is folded on a weakly allowed region ($\phi = \pm180$, $\psi = 0$), implying that the corresponding region in the α,θ plane (represented as a small circle around $\alpha = 0$, $\theta \simeq \tau$) is not strictly forbidden. The effect of the folding along the ϕ,ψ diagonal can also be seen on the core regions of the right-handed (green) and left-

Mapping All-Atom Models

J. Chem. Theory Comput., Vol. 2, No. 3, 2006 **669**
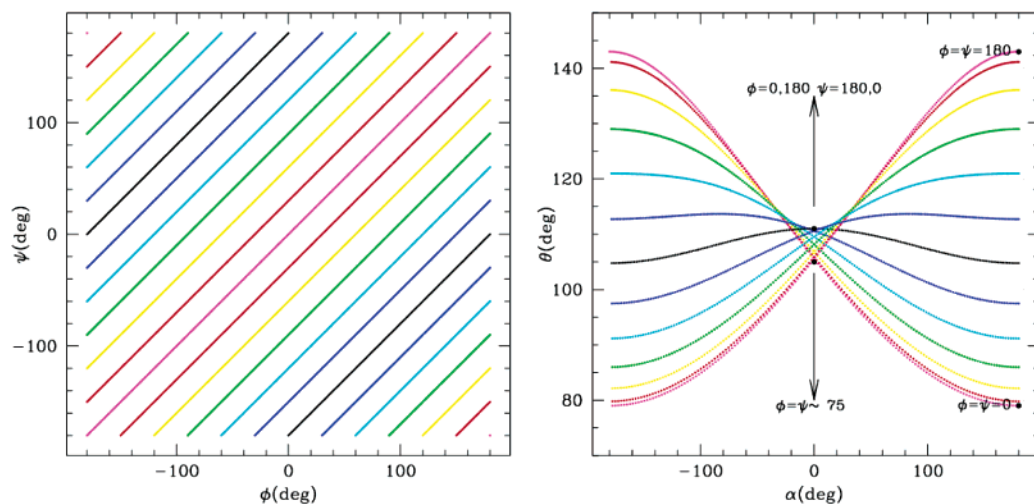
Figure 2. Mapping of the ϕ,ψ plane onto the θ,α plane. Left: lines $\phi - \psi =$ cost are represented in different colors. Right: The same lines are mapped onto the α,θ plane. The region that they define is the image of the whole ϕ,ψ plane onto the α,θ plane through the $(\phi, \psi) \rightarrow (\alpha, \theta)$ map. Some relevant points are reported.
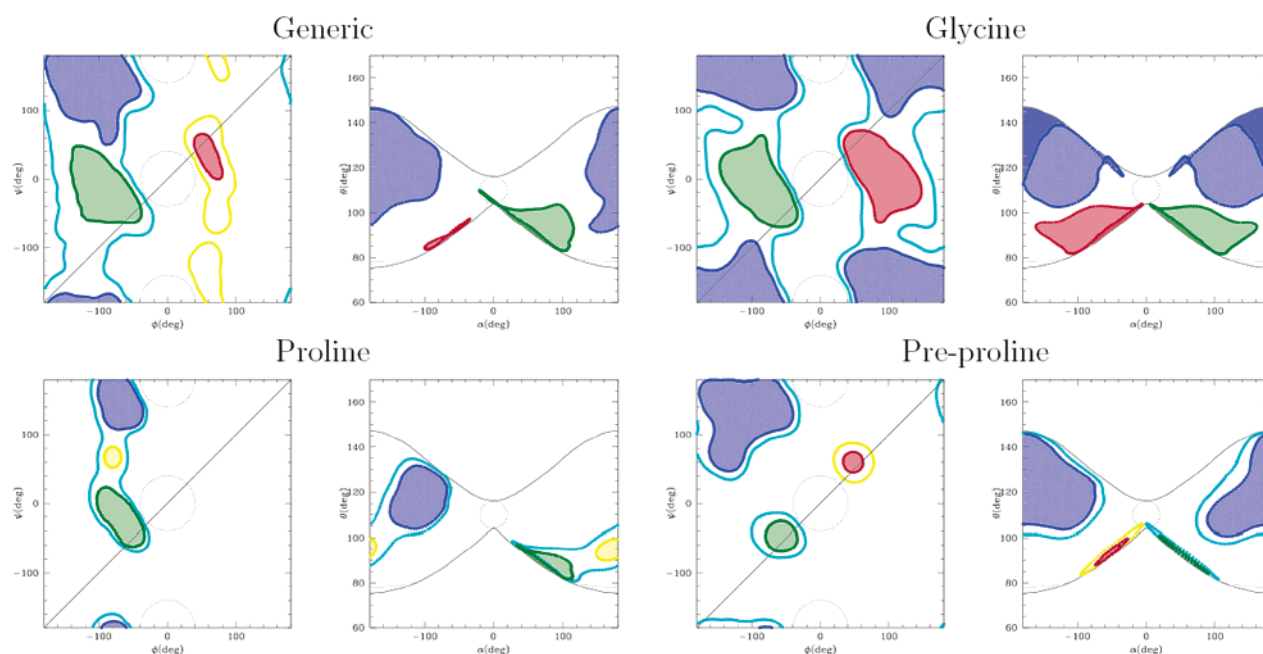
Figure 3. Mapping of the Ramachandran plot onto the α,θ plane for different amino acid types. The "core regions" are in green (right-handed helices), red (left-handed helices), and blue (sheets). The allowed regions (yellow and cyan) are omitted in the generic and glycine α,θ plots for clarity. Forbidden regions are enclosed in the dotted lines. The contours of the "butterfly" image are reported as black lines in the α,θ plane. The input data for the Ramachandran plot are taken from the Protein Data Bank.[18]

handed (red) regions, which are cut by the folding line. These assume peculiar folded and stretched shapes squeezed against the limits of the "butterfly" image. The same happens to the sheet region (blue) in the glycine plot.

However, despite the folding and deformation of the Ramachandran plot, the core regions of the different secondary structures remain separate in the α,θ plane. This is important, because it implies that passing from the ϕ,ψ to the α,θ system of internal coordinates still allows an unambiguous description of the backbone conformation in each secondary structure. This was previously assumed in one- and two-bead CG models but never directly investigated.

In Table 1, the typical ϕ,ψ values for the main secondary structures are reported, as well as the corresponding α,θ values. We observe that right- and left-handed helices have the same value of θ and opposite values of α. Conversely, the θ variable is more efficient in separating the helices from the sheet structures, especially in the glycine where both structures span almost the same α interval.

4. Using the α,θ Plot to Analyze the Force Fields

The potential of mean force $V(q_i)$ is related to the equilibrium probability distribution of the internal coordinate q_i through the relationship $P(q_i) \propto \exp[-V(q_i)/kT]$.

Table 1. Numerical Values of the Internal Angles and Dihedral Coordinates in the All-Atom and CG Representation[a]

structure	ϕ	ψ	θ	α
extended	180	180	146	180
β sheet antiparallel	−139	135	131	179
β sheet parallel ideal	−120	120	121	178
β sheet parallel	−120	113	119	177
flat ribbon	−78	59	92	163
α helix	−57	−47	92	52
3−10 helix	−49	−29	85	81
π helix	−57	−70	99	27
six-membered ring ideal	180	0	115	0
five-membered ring ideal	−75	−75	105	0
five-membered ring	−60	−105	108	0
α helix left-handed	57	47	92	−52
collagen triple helix	−51	153	117	−77
polypro−polygly left helix	−79	150	121	−109

[a] Typical values for secondary structures are reported. Data for ϕ and ψ were taken from textbooks;[19,20] the corresponding structures were built with the *biopolymer* module of Insight (MSI/Accelrys), and from those structures, the θ and α angles were measured.

Although it is well-known that $V(q_i)$ is only an approximation of the potential energy term $U(q_i)$,[21] comparing an approximate probability distribution $p(\alpha,\theta) = \exp[U(\theta,\alpha)/kT]$ to the α,θ plot can still give useful indications.

Very sophisticated $U(\theta,\alpha)$'s are included in the numerical FF derived by Bahar et al.[11,12] and in the UNRES FF by Sheraga et al.,[14,16] which is analytical but involves a very large number of parameters. Here, we analyze the FF with simpler analytical terms. Usually, these include a quite accurate dihedral energy term U^α, with terms in $\sin(n\alpha)$ and $\cos(n\alpha)$ with n up to 6,[3,10] although it was shown that the terms in $\cos(\alpha)$ and $\cos(3\alpha)$ are the most relevant.[8,9,13] In fact, these were included also in the most recent versions of the Gō models.[17] Conversely, the bond angle term $U(\theta)$ is usually treated as harmonic. To include the dependence of the equilibrium θ on the secondary structure, different strategies have been adopted. An explicit correlation $\theta(\alpha)$ was assumed by Levitt,[3] which reduced the dimensionality of the α,θ plot to a line. More realistic α,θ plots can be obtained with an approach like that of Head-Gordon et al.,[8] which uses an accurate dihedral term depending on the amino acid type, reproducing the pattern typical of the helices, sheets, or turns depending on the amino acid type (whose helix−sheet−turn propensity must be known a priori), while a harmonic bond angle term is used with an equilibrium $\theta_0 = 105°$ that is an average of the typical helix and sheet values (see Figure 4, left). Alternatively, angle and dihedral energy terms typical for the β sheet were used, and additional terms depending on the second and third neighbor distance along the chain were used to tune the α-helix propensity, such as in Mukherjee and Bagchi[13] (see Figure 4, right). As can be seen from the plots, these FFs may give a quite accurate pattern of the density plot (at least for the dihedral angle) for given secondary structures, but they are not very appropriate in describing situations when the propensity for a given secondary structure is not very well defined. For instance, they are inadequate to describe the α,θ plot for glycine.

5. A New Force Field with an Accurate Bond Angle Interaction

We recently proposed a different approach[15] including an accurate bond angle term U^θ. We use a quartic double-well potential for the bond angle potential:

$$U^\theta = \frac{1}{2}k_\alpha(\theta - \theta_\alpha)^2 + \frac{1}{3}k'(\theta - \theta_\alpha)^3 + \frac{1}{4}k''(\theta - \theta_\alpha)^4$$

where $\theta_\alpha \simeq 90°$ corresponds to the first minimum (typical of the α helix). The other parameters are related to the position of the second minimum θ_β, to the relative stability $\Delta U^\theta = U_\beta^\theta - U_\alpha^\theta$, and to the (left and right) barriers ΔU_α^θ and ΔU_β^θ via the following relations:

$$\Delta = \theta_\beta - \theta_\alpha$$

$$k' = -\frac{k_\beta + 2k_\alpha}{\Delta}$$

$$k'' = \frac{k_\alpha + k_\beta}{\Delta^2}$$

$$\Delta U^\theta = \frac{\Delta^2}{12}(k_\beta - k_\alpha)$$

$$\Delta U_\alpha^\theta = \frac{\Delta^2}{12}\frac{k_\alpha^3}{(k_\alpha + k_\beta)^3}(k_\alpha + 2k_\beta)$$

$$\Delta U_\beta^\theta = \frac{\Delta^2}{12}\frac{k_\beta^3}{(k_\alpha + k_\beta)^3}(k_\beta + 2k_\alpha)$$

The dihedral term was taken as a harmonic (or harmonic cosine) with an equilibrium value depending on the a priori known secondary structure. The (amino acid dependent) parameters were derived through a statistical analysis of crystallographic structures, using the Boltzmann inversion.[15] The α,θ plots for helix-propense (green), sheet-propense (blue), and glycine-like amino acids are reported in Figure 5 (left). The accuracy of these maps is especially evident in the glycine-like pattern, where our force field reproduces the small separation between the helixlike and sheetlike regions, and in the sheet pattern (blue) where the peculiar shape with a small protuberance toward $\theta = 90°$ present in the "generic" map of Figure 3 is reproduced. This FF has proven successful in reproducing the flap opening dynamics in HIV-1 protease, which depends on a very peculiar motion of the glycine-rich flap tips, and its dependence on the mutations in this region.[15,22]

Here, we propose a further improvement of the potential. We combine our double-well U^θ with a cosine-sum U^α similar to the potential of Head-Gordon et al.[8]

$$U^\alpha = A[1 + \cos(\alpha)] + B[1 + \cos(3\alpha)] + C[1 + \cos(\alpha + \pi/4)] + D[1 + \cos(2\alpha)]$$

whose terms have the following meanings. The first has a minimum at $\alpha = 180°$ corresponding roughly to the sheet or extended structures. The second has additional minima at $\alpha = \pm 60°$, corresponding to helical structures. The third
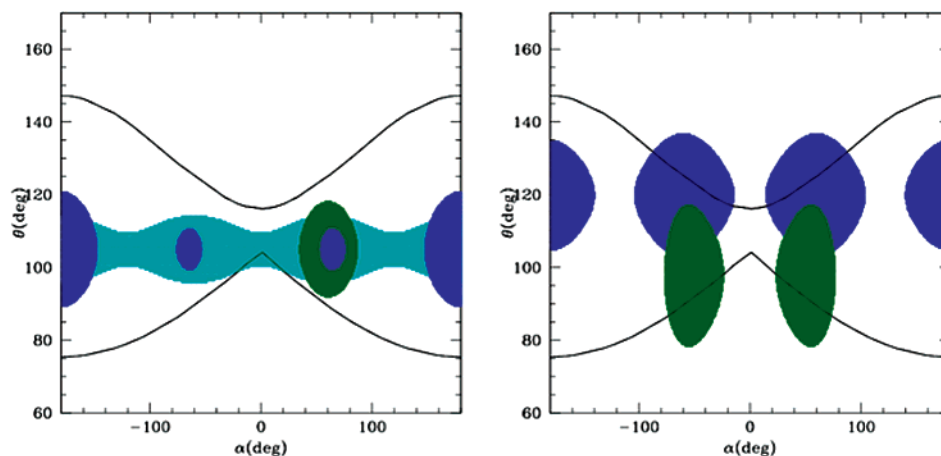
Figure 4. Typical α,θ density maps for two different kinds of FF. Left: Head-Gordon-like FF; right: Mukherjee-like FF. Green, helix; blue, sheet; cyan, turn.
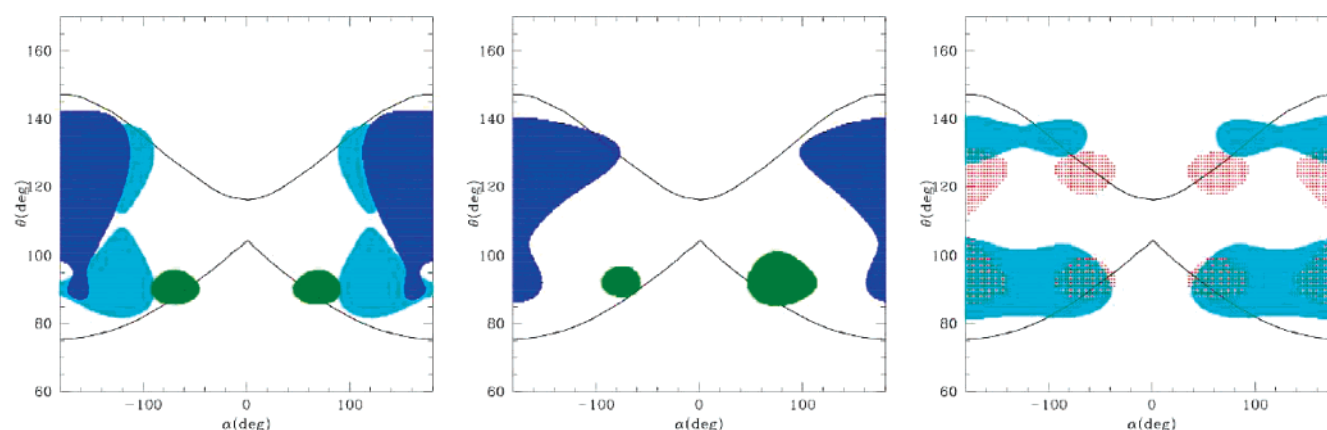
Figure 5. α,θ density maps for the FF in the present work. Left: version with harmonic cosine dihedral potential. Center and right: version with cosine sum dihedral potential. Different maps are obtained giving different weights to the terms, to reproduce the map for sheet (blue), helix (green), glycine (cyan), and generic (red) models.

has a single minimum at $\alpha = 135°$ and introduces an asymmetry that favors the right-handed helices with respect to the left-handed. The fourth has minima at $\alpha = \pm 90°$ and can enforce the helix propensity. By giving different weights to the helixlike or sheetlike terms in U^α and U^θ and tuning the asymmetry term, one can reproduce quite realistic density plots. In Figure 5, in the center, density plots for helixlike (green) and sheetlike (blue) structures are reported. In Figure 5, on the right, we report the density plot for glycine (cyan), obtained using approximately the same weight for the helix and sheet terms and no asymmetry. Finally, in red, we report a hypothetical "generic" potential as simply as possible, including only the first and second terms in U^α. This does not closely resemble any of the "experimental" density plots but contains all the secondary structures with approximately the same weight, also including the very uncommon polyproline helix (located at $\sim 100, \sim 120$) and its right-handed counterpart.

6. Applications: α-Helix to β-Sheet Transition in a Minimal Polypeptide Model

We now illustrate the above concepts with a simple polypeptide model. We do not aim here to describe any specific poly amino acid type; an accurate amino acid type-dependent

parametrization will be the matter of a future paper. However, this model could apply to a sheet former, like polyvaline. In addition to U^α and U^θ, we used a Morse nonbonded interaction potential

$$U^{nb} = \epsilon(\{1 - \exp[-\alpha(r - \sigma)]\}^2 - 1)$$

where $\sigma = 6.1$ Å is the bead diameter, $\alpha = 0.7$ is the well width parameter, and ϵ is taken as an energy unit. Because the helices, sheets, and random coils are characterized by a different number of nonbonded contacts, the relative stability of the different secondary structures depends on a delicate balance between ϵ and $\Delta U^{\alpha,\theta} = \Delta U^\alpha + \Delta U^\theta$. We chose the parameters in such a way that $\Delta U^{\alpha,\theta} = -5\epsilon$ favors the sheet conformation. The energy barriers separating the helix from the sheet were set at $\Delta U^\alpha_\alpha = 6\epsilon$ and $\Delta U^\alpha_\theta = 7\epsilon$, and a slight asymmetry toward the right-handed helix was added to the dihedral potential (see Figure 6 for the values of the parameters). The $C\alpha - C\alpha$ bonds were constrained at the value 3.79 Å. We performed two simulated annealing runs on a 20-mer, starting from the α-helical and extended configurations, respectively. The DL_POLY code was used[23] for the simulation. The results are reported in Figures 6-8.

Figure 7 reports the representative angles and dihedrals along the simulation. In the simulation starting from the α
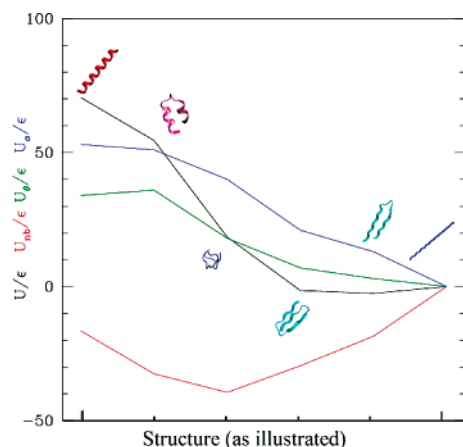
Figure 6. Relative stability and energy terms of the conformations explored during the simulations. Black, total potential energy; red, nonbonded energy; green, bond angle energy; blue, dihedral energy. All energies are expressed in units of ϵ. The extended conformation is taken as the zero level. Parameters of the dihedral and bond angle terms: $A = 2\epsilon$, $B = 4\epsilon$, $C = 0.5\epsilon$, $D = 0$, $\delta U_\alpha^\theta = 7\epsilon$, and $\delta U_\alpha^\theta = 9\epsilon$. Representative structures extracted from the simulations are reported: red, α helix; pink, "broken helix"; violet, random coil; cyan, β hairpin and 3-fold β sheet.
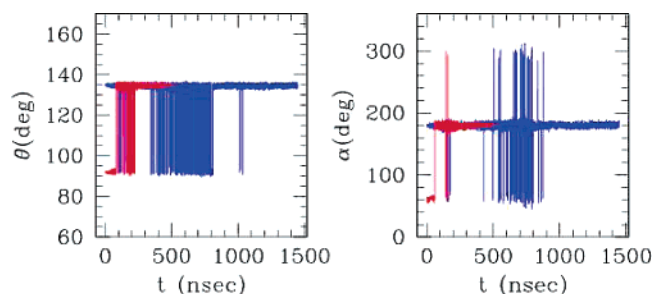
Figure 7. "Representative values" of bond angles and dihedrals evaluated during the simulations starting from the α helix (red) and from the extended structure (blue). The "representative value" is evaluated as follows. For θ, for each time step, all 18 θ angles along the chain are measured, and two average values are calculated, one for the "extended" and one for the "helical" (conventionally separated by the value 113°). The representative value for θ is then chosen as the (average) value of the most populated structure, for each time step. For α, the same procedure is followed, except that in this case three separate average values are calculated for right-handed (between 0 and 115°) or left-handed helices (between −115 and 0°) and for the extended conformation (otherwise).

helix (red), the transition to a globular random coil structure occurs after about 100 ns at the temperature $kT = 0.6\epsilon$, after passing through a metastable "broken helix" conformation (see Figure 6). As the temperature is raised to $kT = \sim\epsilon$, the system explores globular structures, and finally, upon cooling, it stabilizes in a 3-fold β sheet, that is, a β sheet with two β turns located approximately at the 8th and 14th residues along the chain (see Figure 6). In the simulation starting from the extended structure (blue), the system tends to contract to a globule after about 100 ns, then again stabilizes to a 3-fold β sheet. As the temperature is raised to
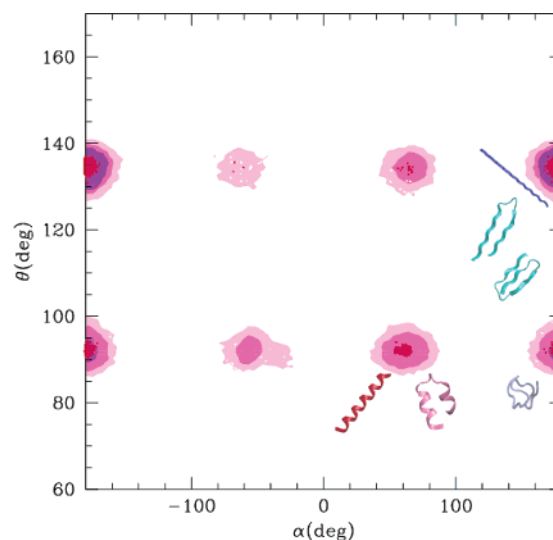
Figure 8. α,θ plot evaluated along the trajectories of the two simulations. Violet: simulation starting from the extended conformation. Pink−magenta−red: simulation starting from the α helix at increasing density values. The representative structures of the populated regions are reported.

$kT \simeq 2\epsilon$ (between 500 and 1000 ns), the system melts into a globular state. During cooling, it explores for long time intervals the β-hairpin structures (β sheets with one β turn approximately in the middle of the chain), before definitely stabilizing in the 3-fold β sheet. Remarkably, the structures we find as (meta)stable states were also observed in simulations performed with more sophisticated models.[24,25]

This dynamical behavior can be explained on the basis of the energy landscape of the system, reported in Figure 6. The energy terms combine in such a way that the helical structures are less stable, while the sheet structures (both β hairpin and 3-fold β sheet) have a very similar energy and are slightly more stable than the extended one. The definitive choice for the 3-fold β sheet may be due to the entropic factor.

The α,θ density plot for the two simulations is shown in Figure 8. The violet map is evaluated on the trajectory of the simulation starting from the extended conformation. Only the area corresponding to the β-sheet and extended structures is populated, with a small population of the globular region located at $\alpha \simeq 180$, $\theta \simeq 90$. The map in red corresponds to the simulation starting from the α helix. The transition to the β sheet passes through the molten globule region; however, as can be seen from the maps obtained with lower levels of populations (magenta and pink), other regions are also (slightly) populated. The pink map resembles the "generic" map (in red in Figure 5), although the effect of the asymmetry term that biases the system toward the "right-handed" structures is evident.

7. Conclusions

In this paper, we have reported two kinds of result. First, we have derived analytical relationships to convert the internal backbone coordinates of the all-atom representation of the polypeptide chain to the internal coordinates of the one- (two-) bead CG representation, namely, the bond angles

and dihedrals θ and α. This result has a general applicability to all cases where the geometry of the backbone must be described and only the coordinates of the Cα's are available, for instance, with low-resolution or CG models. We have used these relationships to convert the Ramachandran plot into new two-dimensional density plots in terms of the backbone variables θ,α. These α,θ density plots can be used as the Ramachandran plot, that is, to test the reliability of protein models, in low-resolution or CG models, when the original Ramachandran plot cannot be used.

Second, we have illustrated these ideas on a minimal one-bead polypeptide model that accounts for the transition from α helices to β sheets. With respect to the models available in the literature, our model contains a more sophisticated bond angle term, which allows one to reproduce quite accurately the α,θ plot. Furthermore, despite its simplicity, this model is shown to explore the conformational space as accurately as more sophisticated multiple-bead models. It is arguable that an optimization and fine-tuning of the parameters of the model can account for the helix or sheet propensities of the different amino acids and reproduce more complex structures and transitions.

Supporting Information Available: The derivation of the exact formula for the dihedral α as a function of ϕ, ψ. This information is available free of charge via the Internet at http://pubs.acs.org.

References

(1) Head-Gordon, T.; Brown, S. *Curr. Opin. Struct. Biol.* **2005**, *13*, 160−167.

(2) Tozzini, V. *Curr. Opin. Struct. Biol.* **2005**, *15*, 144−150.

(3) Levitt, M. *J. Mol. Biol.* **1976**, *12*, 59−107.

(4) Ueeda, Y.; Taketomi, H.; Gō, N. *Biopolymers* **1978**, *17*, 1531−1548.

(5) Nguyen, H. D.; Hall, C. K. *Proc. Natl. Acad. Sci. U.S.A.* **2004**, *101*, 16180−18185.

(6) Fujisuka, Y.; Takada, S.; Luthey-Schulten, Z. A.; Wolynes, P. G. *Proteins* **2004**, *54*, 88−103.

(7) Favrin, G.; Irbäck, A.; Wallin, S. *Proteins* **2002**, *47*, 99−105.

(8) Brown, S.; Fawzi, N. J.; Head-Gordon, T. *Proc. Natl. Acad. Sci. U.S.A.* **2003**, *100*, 10712−10717.

(9) Friedel, M.; Shea, J.-E. *J. Chem. Phys.* **2004**, *120*, 5809−5823.

(10) McCammon, J. A.; Northrup, S. H.; Karplus, M.; Levy, R. M. *Biopolymers* **1980**, *19*, 2033−2045.

(11) Keskin, O.; Bahar, I. *Folding Des.* **1998**, *3*, 469−479.

(12) Bahar, I.; Jernigan, R. L. *J. Mol. Biol.* **1997**, *166*, 195−214.

(13) Mukherjee, A.; Bagchi, B. *J. Chem. Phys.* **2004**, *120*, 1602−1612.

(14) Pillardi, J.; Czaplewski, C.; Liwo, A.; Lee, J.; Ripoll, D. R.; Kazmierkiewicz, R.; Ołdziej, S.; Vedemeyer, W. J.; Gibson, K. D.; Arnautova, Y. A.; Saunders, J.; Ye, Y.-J.; Sheraga, H. A.; *Proc. Natl. Acad. Sci. U.S.A.* **2001**, *98*, 2329−2333.

(15) Tozzini, V.; McCammon, J. A. *Chem. Phys. Lett.* **2005**, *413*, 123−128.

(16) Zacharias, M. *Protein Sci.* **2003**, *12*, 1271−1282.

(17) Koga, N.; Takada, S. *J. Mol. Biol.* **2001**, *313*, 171−180.

(18) RCSB Protein Data Bank. http://pdbbeta.rcsb.org/pdb/.

(19) Mathews, C. K.; van Holde, K. E.; Ahern, K. G. In *Biochemistry*; Addison-Wesley Longman Inc: Reading, MA, 2000; Benjamin−Cummings series.

(20) Voet, D.; Voet J. G. In *Biochimica*; Zanichelli: Bologna, Italy, 1997.

(21) Reith, D.; Pütz, M.; Müller-Plate, F. *J. Comput. Chem.* **2003**, *24*, 1624−1636.

(22) Chang, C.-E.; Shen, T.; Trylska, J.; Tozzini, V.; McCammon, J. A. *Biophys. J.* in press.

(23) Smith, W.; Forester, T. R. *J. Mol. Graphics* **1996**, *14*, 136. Smith, W.; Yong, C. M.; Rodger, P. M. *Mol. Simul.* **2002**, *28*, 385.

(24) Ding, F.; Borreguero, J. M.; Buldyrey, S. V.; Stanley, H. E.; Dokholyan, N. V. *Proteins* **2003**, *53*, 220−228.

(25) Nguyen, H. D.; Marchut, A. J.; Hall, C. K. *Protein Sci.* **2004**, *13*, 2909−2924.